Proton pairing in neutron stars from chiral effective field theory

Yeunhwan Lim[1,2,3,*] and Jeremy W. Holt[4,5]

[1]*Max-Planck-Institut für Kernphysik, Saupfercheckweg 1, 69117 Heidelberg, Germany*
[2]*Institut für Kernphysik, Technische Universität Darmstadt, 64289 Darmstadt, Germany*
[3]*ExtreMe Matter Institute EMMI, GSI Helmholtzzentrum für Schwerionenforschung GmbH, 64291 Darmstadt, Germany*
[4]*Cyclotron Institute, Texas A&M University, College Station, Texas 77843, USA*
[5]*Department of Physics and Astronomy, Texas A&M University, College Station, Texas 77843, USA*

We study the $^1S_0$ proton pairing gap in β-equilibrated neutron star matter within the framework of chiral effective field theory. We focus on the role of three-body forces, which strongly modify the effective proton-proton spin-singlet interaction in dense matter. We find that three-body forces generically reduce both the size of the pairing gap and the maximum density at which proton pairing may occur. The pairing gap is computed within Bardeen-Cooper-Schrieffer theory using a single-particle dispersion relation calculated up to second order in perturbation theory. Model uncertainties are estimated by varying the nuclear potential (its order in the chiral expansion and high-momentum cutoff) and the choice of single-particle spectrum in the gap equation. We find that a second-order perturbative treatment of the single-particle spectrum suppresses the proton $^1S_0$ pairing gap relative to the use of a free spectrum. We estimate the critical temperature for the onset of proton superconductivity to be $T_c = (3.2–5.1) \times 10^9$ K, which is consistent with previous theoretical results in the literature and marginally within the range deduced from a recent Bayesian analysis of neutron star cooling observations.

I. INTRODUCTION

Neutron superfluidity and proton superconductivity play important roles in the physics of neutron stars [1]. The dilute gas of neutrons in the inner crust of a neutron star is expected to pair in the spin-singlet channel, resulting in a neutron superfluid whose vortices provide a large angular momentum reservoir critical for the production of pulsar glitches [2–5]. At the higher densities present in the core of neutron stars, the proton fraction is much less than that of neutrons, and therefore the proton Fermi momentum is not comparable with the neutron Fermi momentum and the formation of neutron-proton Cooper pairs is unlikely. It is then natural to consider neutron-neutron and proton-proton pairing separately. At large densities, neutrons may be paired in the spin-triplet channel, leading to novel cooling processes involving pair formation/breaking that can impact the early thermal evolution of neutron stars [6–14]. Neutron star cooling may also be affected by the presence of superconducting protons in neutron star cores [15,16], though the critical temperature is expected to be somewhat larger than that for neutron superfluidity and consequently would impact the cooling curve at earlier timescales. Well below the critical temperature for neutron superfluidity and proton superconductivity, neutrino emission involving neutrons or protons is highly suppressed due to the minimum gap energy required to break a Cooper pair [17]. Superfluidity also gives reduction

factors to the heat capacity and thermal conductivity of dense nuclear matter [8,18]. Besides neutrino emission from Cooper pairs, superfluidity and superconductivity in the crust and core affect pulsar glitches [19,20], vortex pinning [21,22], and neutron star precession [23,24].

Accurate estimates for nuclear pairing gaps in the various spin and isospin channels are challenging due to uncertainties in strong interaction physics, in particular poorly constrained nuclear many-body correlations and three-body forces that become increasingly important at high densities. In the past, neutron spin-singlet pairing in pure neutron matter has been widely studied, with recent work focusing on the role of three-body forces [25,26] and long- and short-range correlations [27,28] in the Bardeen-Cooper-Schrieffer (BCS) approximation. Quantum Monte Carlo calculations [29], on the other hand, can explore neutron pairing in the strong superfluid regime and connections to ultracold Fermi gases at unitarity. In nearly all cases, however, lattice effects and the presence of nuclear clusters in the neutron star crust are neglected in microscopic many-body calculations of the neutron $^1S_0$ pairing gap. Spin-triplet pairing of neutrons in the neutron star core is anticipated from the strong attraction in the $^3P_2$-$^3F_2$ partial-wave channel observed in nucleon-nucleon (NN) elastic scattering [30]. However, many-body effects such as screening, short-range correlations, and three-body forces play a substantial role, and there is currently much uncertainty in estimates of the spin-triplet pairing gap (for a recent review, see Ref. [31]).

Previous works [32–37] studying proton pairing in neutron star cores have employed a variety of NN interaction models

*ylim@theorie.ikp.physik.tu-darmstadt.de

and many-body methods. The peak in the proton pairing gap was found to vary between $\Delta \simeq 0.4$–0.9 MeV and to occur around normal nuclear densities $n_0 \simeq 0.16$ fm^{-3}, though the density of protons is one or two orders of magnitude less and set by the condition of β equilibrium. More recently [38] a three-body force based on π and ρ meson exchange was included in the solution of the BCS gap equation and found to reduce by half the maximum value of the proton pairing gap compared to the inclusion of two-body forces alone. The two-body force employed in Ref. [38] was the Argonne v_{18} potential, which includes explicit one-pion exchange at large distances but treats the medium- and short-range parts of the NN potential in terms of parametrized phenomenological functions.

In the present study we focus on a microscopic description of proton pairing in neutron star cores employing a set of two- and three-body nuclear forces [39–43] derived in the framework of chiral effective field theory [44–46]. Previous works employing these potentials have shown that they provide a good description of nuclear matter saturation [42,43], the liquid-gas phase transition [47–49], nucleon-nucleus optical potentials [50,51], and Fermi liquid parameters [52]. In addition the derived nuclear equation of state (EOS) is consistent with other studies [53–57] employing different chiral nuclear forces and many-body methods. The present work will be important for developing consistent modeling of the equation of state and nucleonic pairing needed for neutron star cooling calculations.

The paper is organized as follows. In Sec. II we describe the method employed to solve the BCS gap equation. We also detail the treatment of the proton-proton effective interaction and the proton single-particle potential in neutron-rich matter from chiral effective field theory. In Sec. III we present results for the density-dependent $^1S_0$ proton pairing gap at the Fermi surface in beta-equilibrated nuclear matter. Theoretical uncertainties are estimated by varying the resolution scale of the nuclear potential, the order in the chiral expansion, and the treatment of the single-particle dispersion relation. We conclude with a summary and outlook.

II. PROTON PAIRING GAPS IN NEUTRON-RICH MATTER

A. BCS gap equation

The $^1S_0$ pairing gap for a given baryon number density can be obtained in the BCS approximation by solving the gap equation

$$\Delta(k) = -\frac{1}{2} \sum_{k'} V_{\text{eff}}(k, k') \frac{\Delta(k')}{\sqrt{(e_{k'} - \mu)^2 + \Delta^2(k')}}, \quad (1)$$

where $\Delta(k)$ is the pairing gap for the momentum k, $V_{\text{eff}}(k, k')$ is the effective potential between two incoming particles with relative momentum k and outgoing relative momentum k'. The single-particle energy as a function of momentum k is denoted by e_k, and μ is the chemical potential for protons at a given density. In the BCS approximation, the effective potential is chosen as the free-space nucleon-nucleon interaction V_{NN}. Improved approximations account for medium effects, such as three-body force contributions to the in-medium NN

interaction V_{NN}^{med}, as well as long-range correlations and polarization effects. In the present work, we will consider only the additional contributions to $V_{\text{eff}}(k, k')$ from three-body forces. Extensions to include polarization effects through the Fermi liquid theory quasiparticle interaction [28,58,59] will be studied in later work.

Many BCS calculations in nuclear matter employ an effective mass approximation

$$e_k = \frac{k^2}{2M^*} + U, \quad (2)$$

where U depends on the density but is independent of the momentum k. From Eq. (2), the gap equation is then approximated by substituting

$$e_k - \mu \simeq \frac{1}{2M^*}(k^2 - k_F^2). \quad (3)$$

The above approximation assumes that the single-particle energy is nearly quadratic in k near the Fermi momentum k_F. In this case the numerical solution for Eq. (1) can be obtained from a generalized matrix eigenvalue solution [60] by noting that $\Delta_i = F_{ij}\Delta_j$ as in the gap Eq. (1). In practice one applies an adaptive mesh point scheme that depends on the effective mass for a given Fermi momentum.

We also employ the modified Broyden method [61] to verify our numerical solutions. In this approach the gap solution is obtained from a version of direct iteration, where an initial guess of the momentum-dependent gap function is inserted into the right-hand side of Eq. (1) to obtain an updated guess for the gap function on the left-hand side of Eq. (1). The modified Broyden method uses a numerically efficient algorithm for computing and storing the Jacobian, from which the gap equation can be solved iteratively using a pseudo-Newton convergence method (see Refs. [61,62] for complete details). We find that this method converges rapidly once we have an initial guess for the gap size $\Delta(k)$. Moreover, the solution is not particularly sensitive to the initial guess $\Delta^{(0)}(k)$. We find that both methods agree within 1 keV when we use the effective mass approximation in Eq. (2).

The numerical solution to the generalized matrix eigenvalue problem, however, is not applicable when we use a general single-particle energy spectrum instead of the effective mass approximation. The matrix eigenvalue method enables us to obtain an analytic solution for the denominator in Eq. (1), $\sqrt{(e_{k'} - \mu)^2 + \Delta^2(k')}$, when we apply the effective mass approximation. When the single particle energy spectrum does not actually follow a quadratic approximation, the different momentum-dependent effective masses give different gap sizes even though the order of magnitude is similar for each effective mass. Thus, we implement the Broyden method technique as explained in Drischeler *et al.* [62] to obtain the BCS solution in this work.

B. Nucleon single-particle energy

The single-particle energy spectrum plays an important role in determining the solution to the gap equation, and in the present work we consider three approximations to estimate the associated theoretical uncertainty. First, we assume
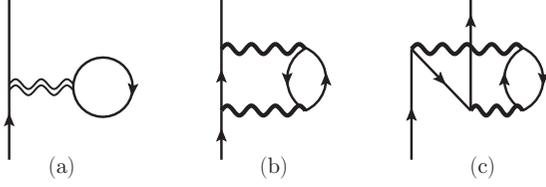
FIG. 1. Diagrammatic contributions to the nucleon self-energy in nuclear matter. The wavy line represents a medium-dependent effective *NN* interaction derived from two- and three-body chiral forces in isospin-asymmetric nuclear matter.

a free-particle spectrum given by $e_k^{(0)} = k^2/2M$. Second, we compute the proton single-particle energy in the Hartree-Fock approximation

$$e_k^{(1)} = k^2/2M + \Sigma^{(1)}(k), \qquad (4)$$

where the first-order contribution $\Sigma^{(1)}(k)$ to the nucleon self energy is shown diagrammatically in Fig. 1(a). Third, we compute the single-particle energy self-consistently at second-order in perturbation theory

$$e_k^{(2)} = k^2/2M + \Sigma^{(1)}(k) + \mathrm{Re}\,\Sigma^{(2)}\big(e_k^{(2)}, k\big), \qquad (5)$$

where $\Sigma^{(2)}(e_k, k)$ is represented by the sum of diagrams (b) and (c) in Fig. 1. The first- and second-order diagrammatic contributions to the nucleon self-energy have the form

$$\Sigma_t^{(1a)}(k) = \sum_1 \langle \vec{k}\,\vec{h}_1 ss_1 tt_1 | \big(\bar{V}_{NN} + \bar{V}_{NN}^{\mathrm{med}}/2\big)|\vec{k}\,\vec{h}_1 ss_1 tt_1\rangle n_1,$$
$$(6)$$

$$\Sigma_t^{(2b)}(k,\omega) = \frac{1}{2}\sum_{123} \frac{|\langle \vec{p}_1 \vec{p}_3 s_1 s_3 t_1 t_3 | \bar{V}_{\mathrm{eff}} | \vec{k}\,\vec{h}_2 ss_2 tt_2\rangle|^2}{\omega + \epsilon_2 - \epsilon_1 - \epsilon_3 + i\eta} \bar{n}_1 n_2 \bar{n}_3,$$
$$(7)$$

$$\Sigma_t^{(2c)}(k,\omega) = \frac{1}{2}\sum_{123} \frac{|\langle \vec{h}_1 \vec{h}_3 s_1 s_3 t_1 t_3 | \bar{V}_{\mathrm{eff}} | \vec{k}\,\vec{p}_2 ss_2 tt_2\rangle|^2}{\omega + \epsilon_2 - \epsilon_1 - \epsilon_3 - i\eta} n_1 \bar{n}_2 n_3,$$
$$(8)$$

where t labels the isospin quantum number of the external particle, $n_j = \theta(k_f - |\vec{p}_j|)$ is the zero-temperature momentum distribution function, $\bar{n}_j = 1 - n_j$, $\bar{V} = V - \mathcal{P}_{12}V$ is the antisymmetrized *NN* potential with $\mathcal{P}_{12}$ the exchange operator, and all sums are taken over momentum, spin, and isospin states.

The effective interaction in Eqs. (8) and (9) is defined by $V_{\mathrm{eff}} = V_{NN} + V_{NN}^{\mathrm{med}}$, where V_{NN}^{med} is the density-dependent *NN* potential derived from the N2LO chiral three-body force by averaging one state over the filled Fermi sea of noninteracting protons and neutrons in asymmetric nuclear matter [63] (for additional details see Refs. [25,64]). In computing the in-medium interaction V_{NN}^{med}, we effectively normal order with respect to a noninteracting (unpaired) ground state. The inclusion of pairing correlations in the normal-ordering reference state for V_{NN}^{med} [65] amounts to summing the third particle over a single-particle BCS spectrum but which otherwise leads to a gap equation that has the same structure as Eq. (1).

The double-wavy line in Fig. 1(a) represents the fact that in the first-order Hartree-Fock contribution to the nucleon self-energy, there is an additional symmetry factor of $\frac{1}{2}$ for the medium-dependent potential, namely, $V_{\mathrm{eff}}^{\mathrm{HF}} = V_{NN} + \frac{1}{2}V_{NN}^{\mathrm{med}}$. The effective interaction in the BCS gap equation, Eq. (1), however, requires no additional symmetry factor [62]. We note that V_{NN}^{med} depends on both the density and composition, namely, the proton fraction. The proton fraction is determined by enforcing β equilibrium, which requires computing the proton and neutron chemical potentials from the equation of state of asymmetric nuclear matter [57,66]. The electrons are treated as a relativistic gas of noninteracting Fermions.

We employ chiral nucleon-nucleon interactions at next-to-next-to-leading order (N2LO) and next-to-next-to-next-to-leading order (N3LO) in the chiral power counting. For values of the momentum-space cutoff $\Lambda \lesssim 500$ MeV, nucleon-nucleon potentials generally exhibit good convergence properties in many-body perturbation theory. In the present work we therefore consider two values of the cutoff ($\Lambda = 450$ MeV and 500 MeV) at N2LO and three values of the cutoff ($\Lambda = 414$ MeV, $\Lambda = 450$ MeV, and 500 MeV) at N3LO [40]. We note that the value $\Lambda = 414$ MeV is not the result of fine tuning but instead corresponds to the relative momentum for nucleon-nucleon scattering at a laboratory energy of $E_{\mathrm{lab}} = 350$ MeV, the maximum energy at which modern nucleon-nucleon potentials are fitted to phase shifts. In all cases we include also the N2LO chiral three-body force whose low-energy constants c_D and c_E are fitted to reproduce the binding energies of $A = 3$ nuclei and the β-decay lifetime of ^{3}He [42,43]. We note that in all cases we employ the charge-dependent versions of these potentials that differ primarily in the leading-order low-energy constant associated with the $^1S_0$ partial wave.

The same approximations for the single-particle energy employed in the present work have been shown to give a good description of the nucleon-nucleus optical potential, especially the dependence of the real part on the isospin asymmetry and energy [67,68]. As we demonstrate below, the many-body perturbation series expansion of the single-particle energies appears to be under control, but uncertainties persist. Despite the above consistencies in the treatment of the effective interaction and single-particle spectrum, additional many-body effects beyond the BCS mean field approximation are important. In particular, both short- and long-range correlations lead to a fragmentation of single-particle strength, encoded in nuclear spectral functions, that modify the quasiparticle energy spectrum. While such effects are partly accounted for through our use of the single-particle energy at second order in perturbation theory, Eq. (5), a complete treatment involving the superfluid Green's function involves a more complicated double energy convolution of the spectral function [69]. Short-range correlations have been shown [28] to reduce by about 25% the size of the neutron pairing gap in the spin-singlet channel. Long-range correlations in the effective pairing interaction, which represent the exchange of virtual collective modes, tend to decrease the strength of the singlet pairing gap by about 20% or less on average for a range of nuclear interactions and densities [28].
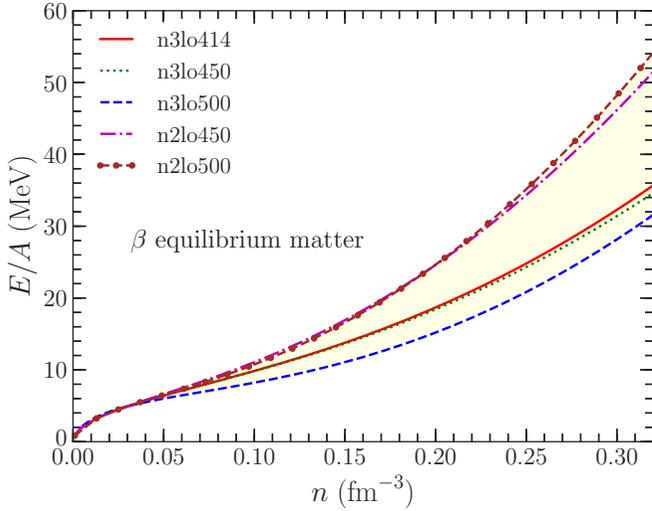
FIG. 2. Equation of state of nuclear matter in beta equilibrium from the chiral two- and three-nuclear forces used in this work.

FIG. 3. Proton fraction as a function of density for β-equilibrated nuclear matter for $n \geqslant 0.5n_0$. Results are shown for the five density-dependent nuclear interactions at N2LO and N3LO.

III. RESULTS

In Fig. 2 we show the equation of state of beta equilibrated nuclear matter calculated from the five chiral nuclear forces employed in the present work. We first compute the equation of state for isospin-asymmetric nuclear matter at second order in perturbation theory:

$$\mathcal{E}^{(1)} = \frac{1}{2}\sum_{12} n_1 n_2 \langle 12 | \left(\bar{V}_{NN} + \bar{V}_{NN}^{\mathrm{med}}/3\right) | 12 \rangle, \qquad (9)$$

$$\mathcal{E}^{(2)} = -\frac{1}{4}\sum_{1234} |\langle 12 | \bar{V}_{\mathrm{eff}} | 34 \rangle|^2 \frac{n_1 n_2 \bar{n}_3 \bar{n}_4}{e_3 + e_4 - e_1 - e_2}, \quad (10)$$

where $\mathcal{E} = E/V$ is the energy density and the single-particle energies e_i in $\mathcal{E}^{(2)}$ are computed according to Eq. (4). Analogous to the calculation of the nucleon self energy in the previous section, the in-medium nucleon-nucleon interaction V_{NN}^{med} requires an additional symmetry factor of 1/3 in the calculation of the Hartree-Fock contribution to the energy density.

From Eqs. (9) and (10), the proton and neutron chemical potentials can be evaluated as

$$\mu_p = \left.\frac{\partial \mathcal{E}}{\partial n_p}\right|_{n_n}, \qquad \mu_n = \left.\frac{\partial \mathcal{E}}{\partial n_n}\right|_{n_p}, \qquad (11)$$

where n_p is the proton number density and n_n is the neutron number density. The electron density is set by charge neutrality, and β equilibrium is then found by enforcing $\mu_n = \mu_p + \mu_e$. As a practical approach, we fit an energy density functional that is consistent with the chiral effective field theory neutron matter and symmetric nuclear matter equations of state from many-body perturbation theory. We have verified that this introduces no significant error in computing the chemical potentials. Strictly speaking, our perturbation theory treatment of the equation of state and single-particle potential does not constitute a conserving approximation, which means that there is some ambiguity in the definition of the chemical potential. Nevertheless, we find good numerical agreement

between the chemical potentials computed from Eq. (11) and from the single-particle energy at the Fermi surface up to a proton Fermi momentum of $k_F^p = 0.6$ fm^{-1}, corresponding to a density of about $1.5n_0$. At higher densities we find that the consistency begins to break down, reaching deviations of about 10% at $2n_0$ at which point the pairing gap vanishes.

As observed in Ref. [43] the energy per particle from the two N2LO chiral potentials is systematically larger than that from the three N3LO potentials, and this difference grows as the density increases. We anticipate a corresponding increase in the $^1S_0$ proton pairing gap uncertainty band for densities $n \gtrsim n_0$. Beyond $n = 2n_0$ a description of the nuclear equation of state based on chiral effective field theory is likely unreliable for the low-momentum perturbative potentials considered in the present work. All results shown below are therefore restricted to the regime $n \leqslant 2n_0$.

At low densities the results for the nuclear equation of state shown in Fig. 2 are in better agreement for the different potentials. However, below $n \lesssim 0.5n_0$ protons in the neutron star inner crust are confined in nuclei and therefore do not form a macroscopic superconductor. Recently it was shown [70] that the crust-core transition density n_t at which unbound protons appear lies in a limited range of $n_t \simeq 0.082$–0.089 fm^{-3} for the three N3LO chiral potentials considered in the present work. The transition density was identified employing two different methods: (i) comparing the ground state energies of the homogeneous and inhomogeneous phase as a function of density in the Thomas-Fermi approximation and (ii) the thermodynamic instability method [71] where the density of homogeneous matter is lowered until an instability to cluster formation appears. Given the tight range of crust-core transition densities found in Ref. [70], we consistently take $n_t \geqslant 0.5n_0$ as the region above which proton pairing may occur.

In Fig. 3 we plot the proton fraction of nuclear matter in beta equilibrium as a function of density for the five nuclear force models considered. We show only densities greater

than $n \geqslant 0.5n_0$ as explained above. Nearly all of the nuclear potentials give consistent predictions for the proton fraction below $n < n_0$, except for the n3lo500 chiral potential which has been shown [72] to exhibit relatively slow convergence in many-body perturbation theory. The proton fraction in nuclear matter depends on the nuclear symmetry energy and its density dependence. For the n3lo500 potential the nuclear symmetry energy is $S_v \simeq 25$ MeV [72] when only the first- and second-order perturbative contributions to the equation of state are included, which is significantly smaller than the values $S_v = 30$–33 MeV for the other potentials considered. Third-order perturbative contributions have been shown [72] to increase the nuclear symmetry energy by 2–3 MeV for this potential, but systematically including such higher-order terms in the present calculation of the pairing gap would not meaningfully alter the final results. In all cases the values of the symmetry energy S_v and its slope parameter L are within the range suggested by Lattimer and Lim [73]. Thus the proton fraction in the β-equilibrated nuclear matter found in this work is consistent with constraints from the most current experimental and theoretical predictions. Beyond nuclear saturation density, the theoretical uncertainty in the proton fraction increases significantly, and higher-order contributions to the symmetry energy become important [74–76]. The two N2LO chiral potentials produce the largest ground-state energy for β-equilibrated nuclear matter and give rise to proton fractions $Y_p = 7.5$–8.5 % at twice saturation density. The three N3LO chiral potentials, on the other hand, predict smaller values of $Y_p = 4$–6 % at $n = 2n_0$.

In Fig. 4 we show the proton and neutron single-particle energies in the Hartree-Fock approximation $e_k^{(1)}$ (top panel) and in the self-consistent second-order approximation $e_k^{(2)}$ (bottom panel) as a function of the momentum k for a specific value of the proton Fermi momentum $k_F^p = 0.4$ fm^{-1}, corresponding to a total baryon number density of $n \simeq 0.5n_0$. This is the density at which the neutron star inner crust transitions to homogeneous nuclear matter in the core, and as we show below it also corresponds to the density at which the proton $^1S_0$ pairing gap is maximal. We see that the inclusion of second-order perturbative corrections to the nucleon self energy leads to a larger isoscalar depth but also a larger isovector splitting between the proton and neutron single-particle energies. Quantitative inspection indicates that whereas the $e_k^{(1)}$ spectrum is nearly quadratic, and hence admits an approximation of the form in Eq. (2), the $e_k^{(2)}$ spectrum deviates strongly from this form in the vicinity of the Fermi momentum. From Fig. 4 we see that the different nuclear potentials give very similar results for the momentum dependence of the proton single-particle energy. As expected for the case of highly neutron-rich matter, the proton single-particle potential is much more strongly attractive than the neutron single-particle potential. In fact, at the proton Fermi momentum $k_F^p = 0.4$ fm^{-1} the proton chemical potential is $\mu_p = e_p(k_F^p) \simeq -65$ MeV.

We next turn our attention to the calculation of the proton pairing gap from Eq. (1). The pairing gap at the Fermi momentum $\Delta(k_F)$ is denoted by Δ_F here and throughout. We first neglect the presence of three-body forces, in which case the nuclear potential is independent of the density and proton fraction, and focus on the role of the single-particle potential,
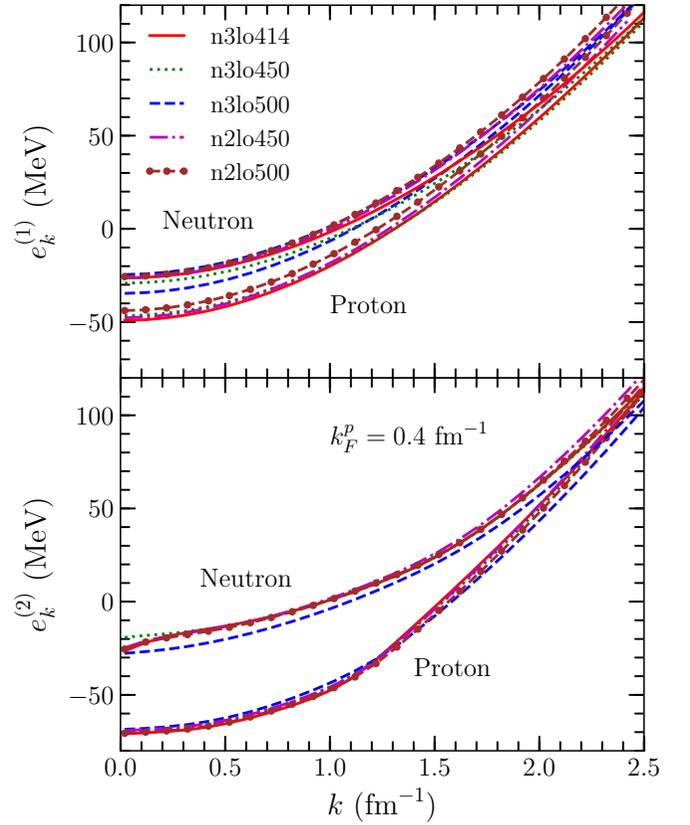
FIG. 4. Single-particle energies as a function of momentum for protons and neutrons in beta-equilibrated nuclear matter at $k_F^p = 0.4$ fm^{-1}. The self-consistent second-order approximation to the single-particle energy, shown in Eq. (5), is employed.

which we parametrize with different choices of the effective mass. In general, the effective mass depends on the density and proton fraction (and also on the momentum when the self energy is computed beyond the Hartree-Fock approximation), but for orientation we consider the case of a constant effective mass. In Fig. 5 we show the proton $^1S_0$ pairing gap from the n3lo450 nucleon-nucleon potential as a function of the proton Fermi momentum for effective masses ranging from $M^*/M = 0.6$–1.0. A free proton spectrum ($M^*/M = 1.0$) gives rise to a maximum in the pairing gap of $\Delta \simeq 3.2$ MeV. Even a moderate reduction in the effective mass to $M^*/M = 0.75$ leads to a decrease in the maximum of the pairing gap by a factor of 2. However, the density at which the pairing gap is maximal decreases by only 10%. The strong dependence of the maximum in the pairing gap on the effective mass can be understood from Eq. (1). A small effective mass corresponds to a strong momentum dependence of the single-particle energy around the Fermi surface. As the intermediate-state momentum in Eq. (1) varies away from the Fermi momentum, the energy denominator increases more rapidly for a small effective mass, reducing the size of the pairing gap.

The effective mass approximation, Eq. (2), provides an accurate parametrization of the nucleon single-particle energy at the Hartree-Fock level. However, second-order perturbative contributions to the nucleon self-energy lead to a strong momentum dependence of the effective mass that is peaked close
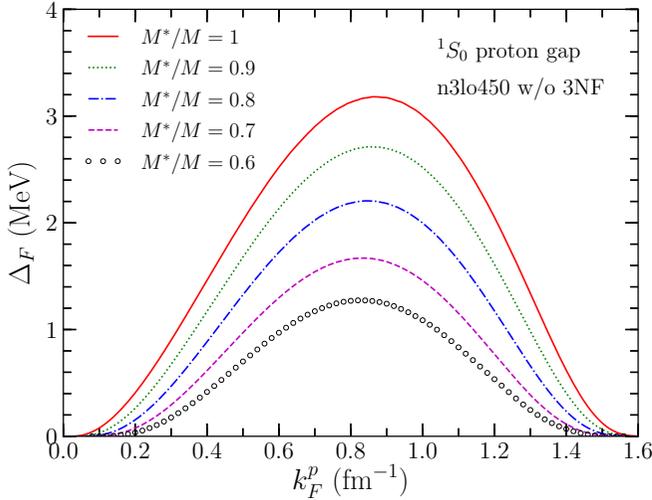
FIG. 5. Density-dependent pairing gap (as a function of the proton Fermi momentum) from chiral two-body forces. The single-particle energies in the gap equation, Eq. (1), are parametrized in terms of a density-independent effective mass M^*.

FIG. 6. Proton-proton pairing gap in β-equilibrated nuclear matter from the n3lo450 chiral nuclear potential, including three-body forces. The dotted vertical line represents the proton Fermi momentum at the neutron star core-crust boundary. Three approximations were employed for the single-particle energy spectrum: (i) free spectrum (dotted line), (ii) Hartree-Fock spectrum (dashed line), and (3) self-consistent second-order spectrum (solid line).

to $M^*/M = 1$ at the Fermi surface [77], the regime where the spectrum most strongly affects the value of the pairing gap. In Table I we show the effective masses at the Fermi surface $k_F^p = 0.4$ fm^{-1} for five different chiral $NN + 3N$ interactions and two choices of the single-particle energy $e_k^{(1)}$ and $e_k^{(2)}$. We see that the second-order perturbative corrections strongly enhance the proton effective mass in comparison to the Hartree-Fock values.

In Fig. 6 we study the effect of different parametrizations of the nucleon single-particle energy on the density-dependent pairing gap. In all cases we include both two- and three-body forces. In the first case, shown as the dotted curve in Fig. 6, we consider a free-particle spectrum $e_k^{(0)} = k^2/2M$. The dotted vertical line stands for the Fermi momentum at the core-crust boundary of a neutron star ($n \sim 1/2n_0$, $Y_p \sim 0.03$). Comparing to Fig. 5 we see that three-body forces lead to a reduction in the maximum value of the pairing gap by a factor of four. Although the proton Fermi momentum is small, the large neutron density leads to a more strongly repulsive effective two-body proton-proton interaction as shown in Ref. [64]. Consequently the maximum proton pairing gap shown in Fig. 6 is roughly $1/3$ the $^1S_0$ neutron pairing gap in neutron star inner crusts [26], where three-body forces play a

TABLE I. Proton effective masses at the Fermi surface $k_F^p = 0.4$ fm^{-1} for different chiral $NN + 3N$ interactions and two choices of the single-particle energy $e_k^{(1)}$ and $e_k^{(2)}$.

V	M_p^*/M_p from $e_k^{(1)}$	M_p^*/M_p from $e_k^{(2)}$
N2LO450	0.76	0.98
N2LO500	0.76	0.97
N3LO414	0.80	0.97
N3LO450	0.82	0.93
N3LO500	0.80	0.87

much smaller role. Treating the single-particle energy in the Hartree-Fock approximation $e_k^{(1)} = k^2/2M + \Sigma^{(1)}(k)$ leads to an additional reduction in the pairing gap by about 40% as shown by the dashed line of Fig. 6. Finally, employing the self-consistent second-order single-particle energy $e_k^{(2)}$ [see Eq. (5)] in the denominator of the gap equation leads to an increase of 20% in the maximum gap size relative to the Hartree-Fock approximation. This may be understood from the fact that the second-order contribution $\Sigma^{(2)}(e_k, k)$ to the self-energy on average increases the effective mass in the vicinity of the Fermi surface.

Figure 7 shows the $^1S_0$ proton pairing gap in the presence of three-body forces using the n3lo450 chiral nuclear potential. The dashed curves correspond to different values of the (fixed) proton fraction Y_p, which ranges from $0.002 \leqslant Y_p \leqslant 0.06$ with $\Delta Y_p = 0.002$, and the solid red curve is that for nuclear matter in beta equilibrium. For a given Y_p we calculate the solution to the BCS gap equation using the first-order approximation for the single-particle energies $e^{(1)}(k)$. We see that the proton fraction is an important parameter for determining the size of the pairing gap. For instance at $k_F^p = 0.4$ fm^{-1}, changing the proton fraction from $Y_p = 0.03$ to $Y_p = 0.04$ would increase the gap size from $\Delta_F = 0.5$ MeV to $\Delta_F = 0.75$ MeV.

We note that the nuclear potential $V_{\rm eff}(k, k')$ depends on the proton fraction when three-body forces are included. As shown in Fig. 7, the proton pairing gap and the available pairing domain in k_F^p increase as the proton fraction increases because $V_{\rm eff}(k, k')$ depends sensitively on the proton fraction. As mentioned in Sec. I, three-body forces have been considered previously in a phenomenological way to compute the proton pairing gap in β-stable nuclear matter. In this work, three-nucleon forces consistent with the low-energy constants
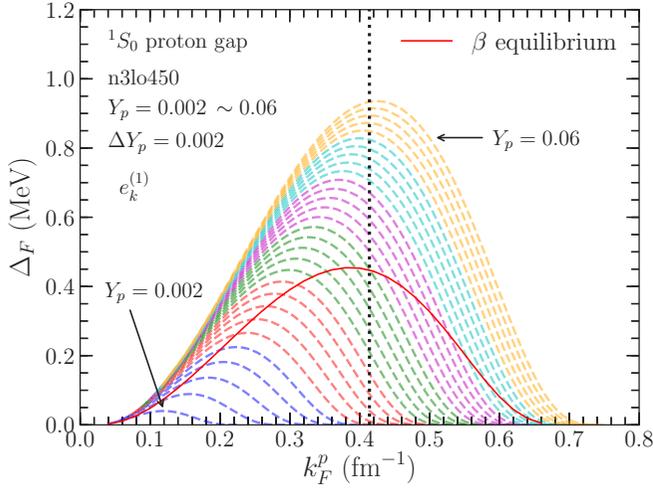
FIG. 7. Density-dependent proton-proton pairing gap from the n3lo450 chiral nuclear potential for different values of the proton fraction Y_p and for nuclear matter in beta equilibrium. A Hartree-Fock single-particle spectrum is employed.

in the two-body force and fitted to the properties of $A = 3$ nuclei have been employed. In addition we have calculated the nuclear EOS with the same nuclear forces to determine the proton fraction.

Figure 8 shows the proton pairing gap in beta-equilibrium matter using five different chiral potentials and two different approximations for the single-particle spectrum: $e_k^{(1)}$ (green) and $e_k^{(2)}$ (red). The dotted sections of the curves indicate the pairing gap for densities lower than that of the neutron star core-crust boundary. The large symbols on the curves indicate the values of the pairing gap at nuclear densities $n = n_0/2$ (open circle), n_0 (filled circle), $3n_0/2$ (open square), and $2n_0$ (filled square). Only the proton pairing gap from the N3LO500 potential using the $e_k^{(2)}$ spectrum does not show closure in k_F^p. This is due to the associated small proton fraction (see Fig. 3), which leads to a larger value of the total baryon
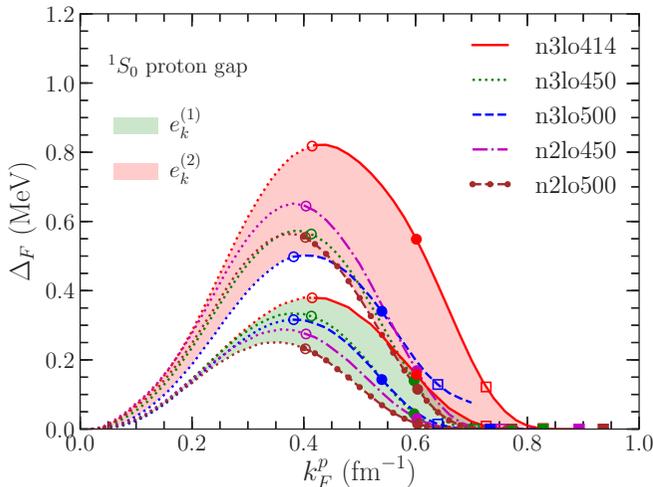
FIG. 8. Proton $^1S_0$ pairing gap as a function of the Fermi momentum k_F for the five chiral potentials considered in the present work.

number density for a given value of k_F^p. We have restricted our calculations to the density regime $n \leqslant 2n_0$ and therefore do not report results for $k_F^p > 0.72$ fm^{-1} from the N3LO500 potential. In particular, just below twice saturation density, the self-consistent calculation of the single-particle potential from the N3LO500 potential begins to break down.

We note several nearly universal features in the results of Fig. 8, independent of the choice of chiral interaction and the associated derived quantities, such as the single-particle spectrum and proton fraction. First, for all cases the peak in the pairing gap occurs very close to the crust-core boundary and within a very small window of the proton Fermi momentum 0.35 fm^{-1} < k_F^p < 0.43 fm^{-1}. Second, apart from the results of the N3LO414 and N3LO500 potentials using the $e_k^{(2)}$ energy spectrum, nearly all potentials lead to a proton pairing gap that vanishes when the proton Fermi momentum is in the range 0.65 fm^{-1} < k_F^p < 0.75 fm^{-1}. Even the inclusion of both the N3LO414 and N3LO500 potentials would only increase the upper bound to $k_F^p \simeq 0.8$ fm^{-1}, which corresponds to a total baryon number density less than $2n_0$. We therefore note that proton pairing is expected to exist within a neutron star at densities where chiral effective field theory is valid.

Chiral potentials generally become more repulsive as the momentum-space cutoff Λ increases, which partly accounts for the smaller proton pairing gaps associated with the N2LO500 and N3LO500 chiral potentials and the largest proton pairing gaps associated with the N3LO414 potential. For neutron matter and beta stable nuclear matter, it was also shown that the N2LO equations of state are stiffer than at N3LO. The effect of repulsive contributions in the nuclear potential are mostly clearly seen in the pairing gaps associated with the $e_k^{(1)}$ spectrum, where there is a clear trend from the N2LO potentials (with the smallest gaps) to the N3LO potentials ordered according to the value of the cutoff Λ. In addition to the EOS stiffness (where an attractive force would increase the gap size and the EOS would be soft), the gap size is also related to the proton fraction in β-equilibrium matter (which controls the proton Fermi momentum), and the proton single-particle spectrum. From Fig. 8 we see that the inclusion of second-order contributions to the single-particle energy has a strong impact on the proton pairing gap. The nucleon effective mass at the Hartree-Fock $e_k^{(1)}$ approximation is small $M^*/M \sim 0.75$, while second-order perturbative contributions lead to a strong energy dependence in the single-particle potential that increases the effective mass to $M^*/M \sim 1$ near the Fermi surface. As can be inferred from Fig. 5, this generically leads to larger proton pairing gaps in Fig. 8 for the $e_k^{(2)}$ spectrum. Specifically, in the $e_k^{(2)}$ approximation we find that the N2LO450, N2LO500, and N3LO414 potentials experience the largest changes in the proton effective mass, which enhances the magnitude of the pairing gap relative to their values with the $e_k^{(1)}$ spectrum. From the above considerations we find that multiple effects strengthen the pairing gap associated with the N3LO414 potential, which explains why it deviates most strongly from the other potentials when the $e_k^{(2)}$ spectrum is employed.

In Fig. 9 we compare the proton pairing gap uncertainty band calculated in the present work to previous results in the literature. We find that employing the $e_k^{(2)}$ approximation
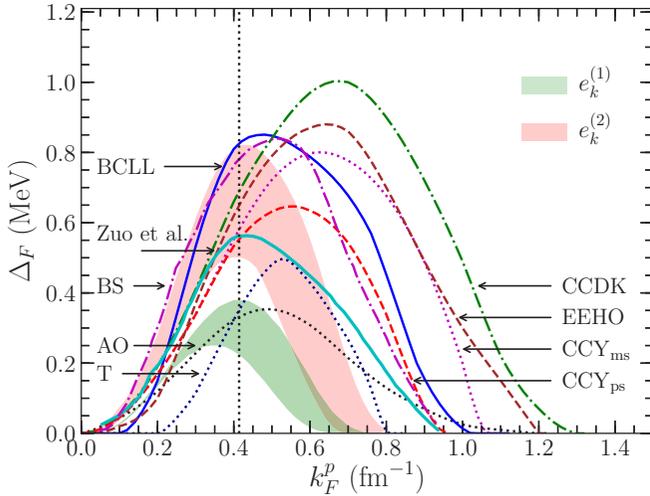
FIG. 9. $^1S_0$ proton pairing curves from nuclear model. Our EFT calculation (red band) gives similar pairing gaps and smaller range of Fermi momentum where the pairing is available. For comparison, it is shown the previous BCS calculations, Chao *et al.* [32] ('CCY'), Takatsuka [33] ('T'), Amundsen and Østgaard [34] ('AO'), Baldo *et al.* [35] ('BCLL'), Chen *et al.* [36] ('CCDK'), Elgarøy *et al.* [37] ('EEHO'), Zuo *et al.* [38] ('Zuo *et al.*'), and Baldo and Schulze [90] ('BS').

for the single-particle spectrum, the maximum in the pairing gap lies in the range $0.51 \text{ MeV} < \Delta_F < 0.82$ MeV, which is consistent with previous calculations, but the maximum density at which proton pairing is expected to occur is systematically smaller than other models. This is largely caused by three-body forces and the behavior of the chiral potential $V_{\text{eff}}(k, k')$ as the proton fraction is increased in neutron star matter. Employing the $e_k^{(1)}$ spectrum we find instead that $0.25 \text{ MeV} < \Delta_F < 0.38$ MeV. The medium-dependent nuclear potential in isospin-asymmetric nuclear matter might also affect to a lesser extent the $^3P_2$ - $^3F_2$ neutron pairing gap, which is typically calculated in pure neutron matter. We note that our error bands in Fig. 9 partially account for uncertainties due to (i) the convergence of the chiral expansion (where we have varied the chiral order of the nucleon-nucleon interaction from N2LO to N3LO), (ii) the choice of the resolution scale at which nuclear dynamics is resolved (encoded in the high-momentum cutoff in the chiral potential), and (iii) the convergence in the many-body expansion (through different choices of the single-particle spectrum). A more comprehensive account of uncertainties would include varying the chiral EFT low-energy constants within ranges consistent with $2N$ and $3N$ scattering data and three-body bound state properties [78,79], improved order-by-order effective field theory truncation errors [80–82] including consistent N3LO three-body forces [83–88], and the improved description of short- and long-range correlations that go beyond the BCS approximation [28,89].

In the weak coupling approximation, the critical temperature for the onset of pairing is given by [91]

$$T_c \simeq 0.57 \, \Delta_F(T = 0). \tag{12}$$
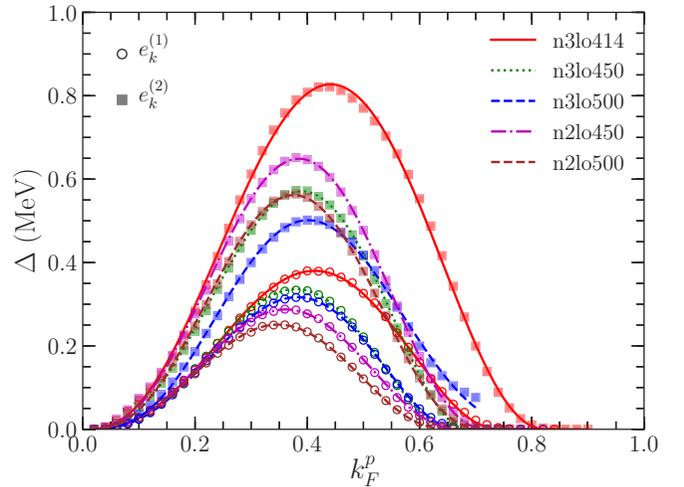
FIG. 10. Calculated proton pairing gaps using the $e_k^{(1)}$ single-particle energy (open symbols) and the $e_k^{(2)}$ single-particle energy (filled symbols) together with the parametrization (solid lines) in Eq. (14).

We find that in the present analysis with the $e_k^{(2)}$ spectrum, the critical temperature for proton pairing in the core of neutron stars is

$$T_c \sim (3.2\text{–}5.1) \times 10^9 \, \text{K} \,. \tag{13}$$

Compared to the range of critical temperatures predicted in a recent study from neutron star cooling using Bayesian analysis [92], where $T_c = 7.59^{+2.48}_{-5.81} \times 10^9$ K, our prediction has a smaller central value but is consistent at the highest range.

Finally, we consider parametrized fitting functions for the pairing gaps shown in Fig. 8. We find that the pairing gap can be well fitted with the simple function [14]

$$\Delta(k_F) = \begin{cases} \Delta_{\text{m}} \mathcal{N} (k_F - k_1)^\alpha (k_2 - k_F)^\beta, & \text{if } k_1 < k_F < k_2 \,, \\ 0, & \text{otherwise} \,, \end{cases} \tag{14}$$

where $\mathcal{N}$ is the normalization factor given by

$$\mathcal{N} = \frac{1}{\alpha^\alpha \beta^\beta} \left(\frac{\alpha + \beta}{k_2 - k_1} \right)^{\alpha + \beta} \,. \tag{15}$$

In Fig. 10 we plot the numerical pairing gaps as well as the fitting functions under the two approximations $e_k^{(1)}$ (open circles) and $e_k^{(2)}$ (filled squares) for the single-particle energies. We see that in all cases the parametrized form in Eq. (14) captures very well the k_F^p dependence of the gaps. In Table II will list the values of the parameters for the different chiral interactions and choices of single-particle spectrum.

IV. SUMMARY

In this work we have studied the proton $^1S_0$ pairing gap in nuclear matter at beta equilibrium using five different nuclear two- and three-body potentials derived within the framework of chiral effective field theory. Nucleon-nucleon potentials at both N2LO and N3LO were considered, together with the chiral three-body force at N2LO. In addition to the choice of

TABLE II. Fitting parameters for the $^1S_0$ proton pairing gap in Eq. (14) for different chiral potentials and choices for the single-particle energy spectrum.

Model	Δ_m (MeV)	k_1 (fm^{-1})	k_2 (fm^{-1})	α	β
$e_k^{(1)}$ n3lo414	0.380	0.000	0.748	2.998	2.432
$e_k^{(1)}$ n3lo450	0.336	0.000	0.663	3.116	2.319
$e_k^{(1)}$ n3lo500	0.317	0.004	0.672	3.041	2.325
$e_k^{(1)}$ n2lo450	0.287	0.000	0.682	3.058	2.713
$e_k^{(1)}$ n2lo500	0.251	0.000	0.658	3.054	2.723
$e_k^{(2)}$ n3lo414	0.827	0.002	0.828	2.769	2.434
$e_k^{(2)}$ n3lo450	0.571	0.000	0.689	2.965	2.275
$e_k^{(2)}$ n3lo500	0.501	0.000	0.860	3.507	4.003
$e_k^{(2)}$ n2lo450	0.649	0.000	0.726	3.019	2.672
$e_k^{(2)}$ n2lo500	0.562	0.000	0.722	3.159	2.914

nuclear potential, also the single-particle spectrum employed in the BCS gap equation is a source of theoretical uncertainty.

We find that both three-body forces and a realistic proton single-particle potential in neutron star matter reduce the maximum size of the proton $^1S_0$ pairing gap. In particular, three-body forces reduce the maximum gap size by a factor of 3, while a self-consistent second-order treatment of the proton single-particle potential leads to an additional reduction of about 30%. Our results for the $^1S_0$ proton pairing gap have a similar range of sizes compared to previous studies. However, the maximum density at which proton pairing may exist in

neutron stars is systematically smaller than previous results. This ultimately comes from the inclusion of three-body forces in our effective field theory calculation, which requires a consistent calculation of the proton fraction in β-equilibrium matter. The three-body force leads to additional repulsion in the effective interaction and a suppression in the pairing gap as the density increases.

These results will be important for a consistent description of neutron star cooling. Proton $^1S_0$ pairing will likely not give any reduction factor for nucleon direct Urca cooling, since the pairing gap is seen to vanish well before the proton fraction reaches a value high enough for the onset of the direct Urca process. However, proton pairing will certainly give a reduction factor to the thermal conductivity, heat capacity, and neutrino emission processes involving protons. Thus the enhanced cooling processes in neutrons stars arising from Cooper-pair breaking/formation is likely to be dominated by $^3P_2$ neutron pairing in the core rather than $^1S_0$ pairing of protons.

[1] D. J. Dean and M. Hjorth-Jensen, Rev. Mod. Phys. **75**, 607 (2003).
[2] G. Baym, C. Pethick, D. Pines, and M. Ruderman, Nature **224**, 872 (1969).
[3] N. Andersson, K. Glampedakis, W. C. G. Ho, and C. M. Espinoza, Phys. Rev. Lett. **109**, 241103 (2012).
[4] N. Chamel, Phys. Rev. C **85**, 035801 (2012).
[5] J. Piekarewicz, F. J. Fattoyev, and C. J. Horowitz, Phys. Rev. C **90**, 015803 (2014).
[6] E. Flowers, M. Ruderman, and P. Sutherland, Astrophys. J. **205**, 541 (1976).
[7] D. Voskresenskii and A. Senatorov, Sov. J. Nucl. Phys. **45**, 411 (1987).
[8] D. G. Yakovlev, K. P. Levenfish, and Yu. A. Shibanov, Phys. Usp. **42**, 737 (1999).
[9] D. Page, J. M. Lattimer, M. Prakash, and A. W. Steiner, Astrophys. J. Suppl. **155**, 623 (2004).
[10] C. O. Heinke and W. C. G. Ho, Astrophys. J. Lett. **719**, L167 (2010).
[11] D. Page, J. M. Lattimer, M. Prakash, and A. W. Steiner, Astrophys. J. **707**, 1131 (2009).
[12] D. Page, M. Prakash, J. M. Lattimer, and A. W. Steiner, Phys. Rev. Lett. **106**, 081101 (2011).
[13] P. S. Shternin, D. G. Yakovlev, C. O. Heinke, W. C. G. Ho, and D. J. Patnaude, Mon. Not. Roy. Astron. Soc. **412**, L108 (2011).
[14] Y. Lim, C. H. Hyun, and C.-H. Lee, Int. J. Mod. Phys. E **26**, 1750015 (2017).
[15] A. D. Kaminker, P. Haensel, and D. G. Yakovlev, Astron. Astrophys. **345**, L14 (1999).
[16] M. E. Gusakov, A. D. Kaminker, D. G. Yakovlev, and O. Y. Gnedin, Astron. Astrophys. **423**, 1063 (2004).
[17] D. Yakovlev, A. Kaminker, O. Gnedin, and P. Haensel, Phys. Rep. **354**, 1 (2001).
[18] D. A. Baiko, P. Haensel, and D. G. Yakovlev, Astron. Astrophys. **374**, 151 (2001).
[19] B. Link, R. I. Epstein, and K. A. Van Riper, Nature **359**, 616 (1992).
[20] W. C. G. Ho, C. M. Espinoza, D. Antonopoulou, and N. Andersson, Sci. Adv. **1**, e1500578 (2015).
[21] M. A. Alpar, D. Pines, P. W. Anderson, and J. Shaham, Astrophys. J. **276**, 325 (1984).
[22] R. I. Epstein and G. Baym, Astrophys. J. **328**, 680 (1988).
[23] B. Link, Phys. Rev. Lett. **91**, 101101 (2003).
[24] K. Glampedakis, N. Andersson, and D. I. Jones, Phys. Rev. Lett. **100**, 081101 (2008).
[25] K. Hebeler and A. Schwenk, Phys. Rev. C **82**, 014314 (2010).
[26] S. Maurizio, J. W. Holt, and P. Finelli, Phys. Rev. C **90**, 044003 (2014).
[27] L. G. Cao, U. Lombardo, and P. Schuck, Phys. Rev. C **74**, 064301 (2006).

[28] D. Ding, A. Rios, H. Dussan, W. H. Dickhoff, S. J. Witte, A. Carbone, and A. Polls, Phys. Rev. C **94**, 025802 (2016).

[29] A. Gezerlis and J. Carlson, Phys. Rev. C **77**, 032801(R) (2008).

[30] V. G. J. Stoks, R. A. M. Klomp, M. C. M. Rentmeester, and J. J. de Swart, Phys. Rev. C **48**, 792 (1993).

[31] A. Gezerlis, C. J. Pethick, and A. Schwenk, in *Novel Superfluids*, edited by K. H. Bennemann and J. B. Ketterson (Oxford University Press, 2014), Vol. 2, p. 580.

[32] N.-C. Chao, J. Clark, and C.-H. Yang, Nucl. Phys. A **179**, 320 (1972).

[33] T. Takatsuka, Prog. Theor. Phys. **50**, 1754 (1973).

[34] L. Amundsen and E. Østgaard, Nucl. Phys. A **437**, 487 (1985).

[35] M. Baldo, J. Cugnon, A. Lejeune, and U. Lombardo, Nucl. Phys. A **536**, 349 (1992).

[36] J. Chen, J. Clark, R. Davé, and V. Khodel, Nucl. Phys. A **555**, 59 (1993).

[37] Ø. Elgarøy, L. Engvik, M. Hjorth-Jensen, and E. Osnes, Nucl. Phys. A **604**, 466 (1996).

[38] W. Zuo, Z. H. Li, G. C. Lu, J. Q. Li, W. Scheid, U. Lombardo, H. J. Schulze, and C. W. Shen, Phys. Lett. B **595**, 44 (2004).

[39] D. R. Entem and R. Machleidt, Phys. Rev. C **68**, 041001(R) (2003).

[40] E. Marji, A. Canul, Q. MacPherson, R. Winzer, C. Zeoli, D. R. Entem, and R. Machleidt, Phys. Rev. C **88**, 054002 (2013).

[41] L. Coraggio, J. W. Holt, N. Itaco, R. Machleidt, and F. Sammarruca, Phys. Rev. C **87**, 014322 (2013).

[42] L. Coraggio, J. W. Holt, N. Itaco, R. Machleidt, L. E. Marcucci, and F. Sammarruca, Phys. Rev. C **89**, 044321 (2014).

[43] F. Sammarruca, L. Coraggio, J. W. Holt, N. Itaco, R. Machleidt, and L. E. Marcucci, Phys. Rev. C **91**, 054311 (2015).

[44] S. Weinberg, Physica A **96**, 327 (1979).

[45] E. Epelbaum, H.-W. Hammer, and Ulf-G. Meißner, Rev. Mod. Phys. **81**, 1773 (2009).

[46] R. Machleidt and D. R. Entem, Phys. Rep. **503**, 1 (2011).

[47] C. Wellenhofer, J. W. Holt, N. Kaiser, and W. Weise, Phys. Rev. C **89**, 064009 (2014).

[48] J. W. Holt, N. Kaiser, and W. Weise, Prog. Part. Nucl. Phys. **73**, 35 (2013).

[49] J. W. Holt, M. Rho, and W. Weise, Phys. Rep. **621**, 2 (2016).

[50] J. W. Holt, N. Kaiser, G. A. Miller, and W. Weise, Phys. Rev. C **88**, 024614 (2013).

[51] J. W. Holt, N. Kaiser, and G. A. Miller, Phys. Rev. C **93**, 064603 (2016).

[52] J. W. Holt, N. Kaiser, and W. Weise, Nucl. Phys. A **876**, 61 (2012).

[53] S. K. Bogner, A. Schwenk, R. J. Furnstahl, and A. Nogga, Nucl. Phys. A **763**, 59 (2005).

[54] K. Hebeler, S. K. Bogner, R. J. Furnstahl, A. Nogga, and A. Schwenk, Phys. Rev. C **83**, 031301(R) (2011).

[55] G. Hagen, T. Papenbrock, A. Ekström, K. A. Wendt, G. Baardsen, S. Gandolfi, M. Hjorth-Jensen, and C. J. Horowitz, Phys. Rev. C **89**, 014319 (2014).

[56] A. Carbone, A. Rios, and A. Polls, Phys. Rev. C **90**, 054322 (2014).

[57] C. Drischler, K. Hebeler, and A. Schwenk, Phys. Rev. C **93**, 054314 (2016).

[58] A. Sedrakian and J. W. Clark, Eur. Phys. J. A **55**, 167 (2019).

[59] J. W. Holt, N. Kaiser, and T. R. Whitehead, Phys. Rev. C **97**, 054325 (2018).

[60] H. H. Fan, E. Krotscheck, T. Lichtenegger, D. Mateo, and R. E. Zillich, Phys. Rev. A **92**, 023640 (2015).

[61] D. D. Johnson, Phys. Rev. B **38**, 12807 (1988).

[62] C. Drischler, T. Krüger, K. Hebeler, and A. Schwenk, Phys. Rev. C **95**, 024302 (2017).

[63] F. Sammarruca, R. Machleidt, and N. Kaiser, Phys. Rev. C **92**, 054327 (2015).

[64] J. W. Holt, N. Kaiser, and W. Weise, Phys. Rev. C **81**, 024002 (2010).

[65] P. Papakonstantinou and J. W. Clark, J. Low Temp. Phys. **189**, 361 (2017).

[66] C. Wellenhofer, J. W. Holt, and N. Kaiser, Phys. Rev. C **92**, 015801 (2015).

[67] T. R. Whitehead, Y. Lim, and J. W. Holt, Phys. Rev. C **100**, 014601 (2019).

[68] T. R. Whitehead, Y. Lim, and J. W. Holt, Phys. Rev. C **101**, 064613 (2020).

[69] A. Rios, A. Polls, and W. Dickhoff, J. Low Temp. Phys. **189**, 234 (2017).

[70] Y. Lim and J. W. Holt, Phys. Rev. C **95**, 065805 (2017).

[71] G. Baym, H. A. Bethe, and C. Pethick, Nucl. Phys. A **175**, 225 (1971).

[72] J. W. Holt and N. Kaiser, Phys. Rev. C **95**, 034326 (2017).

[73] J. M. Lattimer and Y. Lim, Astrophys. J. **771**, 51 (2013).

[74] B.-J. Cai and L.-W. Chen, Phys. Rev. C **85**, 024302 (2012).

[75] W. M. Seif and D. N. Basu, Phys. Rev. C **89**, 028801 (2014).

[76] P. Wen and J. W. Holt, arXiv:2012.02163.

[77] G. F. Bertsch and T. T. S. Kuo, Nucl. Phys. A **112**, 204 (1968).

[78] S. Wesolowski, R. Furnstahl, J. Melendez, and D. Phillips, J. Phys. G **46**, 045102 (2019).

[79] P. Reinert, H. Krebs, and E. Epelbaum, Eur. Phys. J. A **54**, 86 (2018).

[80] E. Epelbaum, H. Krebs, and U. Meißner, Eur. Phys. J. A **51**, 53 (2015).

[81] R. J. Furnstahl, N. Klco, D. R. Phillips, and S. Wesolowski, Phys. Rev. C **92**, 024005 (2015).

[82] C. Drischler, R. Furnstahl, J. Melendez, and D. Phillips, Phys. Rev. Lett. **125**, 202702 (2020).

[83] S. Ishikawa and M. R. Robilotta, Phys. Rev. C **76**, 014006 (2007).

[84] V. Bernard, E. Epelbaum, H. Krebs, and Ulf-G. Meißner, Phys. Rev. C **77**, 064004 (2008).

[85] V. Bernard, E. Epelbaum, H. Krebs, and Ulf-G. Meißner, Phys. Rev. C **84**, 054001 (2011).

[86] I. Tews, T. Krüger, K. Hebeler, and A. Schwenk, Phys. Rev. Lett. **110**, 032504 (2013).

[87] C. Drischler, A. Carbone, K. Hebeler, and A. Schwenk, Phys. Rev. C **94**, 054307 (2016).

[88] J. W. Holt, M. Kawaguchi, and N. Kaiser, Front. Phys. **8**, 100 (2020).

[89] D. Page, J. M. Lattimer, M. Prakash, and A. W. Steiner, arXiv:1302.6626.

[90] M. Baldo and H.-J. Schulze, Phys. Rev. C **75**, 025802 (2007).

[91] E. M. Lifchits and L. P. Pitaevski, *Statistical Physics, Part 2* (Pergamon Press, Oxford, 1980).

[92] S. Beloin, S. Han, A. W. Steiner, and D. Page, Phys. Rev. C **97**, 015804 (2018).